JOURNAL OF AIRCRAFT
Vol. 47, No. 1, January–February 2010

Comparison of Two Kite Force Models with Experiment

George M. Dadd,* Dominic A. Hudson,† and R. A. Shenoi‡
University of Southampton, Southampton, England SO17 1BJ, United Kingdom

DOI: 10.2514/1.44738

Kite propulsion has emerged as an attractive means to harness wind power in a way that yields environmental and financial benefits. This paper compares results from two line tension models with experimentally recorded time histories for dynamic kite flight. New methodologies for investigating kite performance are established. The first zero mass model assumes that the kite and lines are weightless. The second lumped mass model considers the kite's mass and thus, makes use of the equations of motion. It is found that the two different models converge to the same result in the limit where the kite mass tends to zero. Kite mass is shown to affect performance only to a relatively small extent. The zero mass model has been shown to compare favorably with experimental results for the prediction of performance during three-dimensional kite trajectories.

Nomenclature

A_{BL}	=	projected area of lines and bridles, m^2
A_K	=	projected kite area, m^2
AR	=	aspect ratio
$\mathbf{a}_K$	=	acceleration, ms^{-2}
$\mathbf{C}$	=	circumferential component of aerodynamic force, vector, N
C	=	circumferential component of aerodynamic force, magnitude, N
C_D	=	drag coefficient
$C_{D_{BL}}$	=	kite line drag coefficient
C_L	=	lift coefficient
C_T	=	line tension coefficient
$\mathbf{c}$	=	circumferential component of aerodynamic force, unit vector, N
c_k	=	chord of kite, m
$\mathbf{D}$	=	aerodynamic drag force vector, N
D	=	drag force magnitude, N
D_{BL}	=	drag due to bridle and lines, N
$\mathbf{F}$	=	aerodynamic force vector, N
F_A	=	aerodynamic force vector magnitude, N
f, g	=	generic functions
$\mathbf{g}$	=	acceleration due to gravity (taken as 9.81 ms^{-2}), ms^{-2}
L	=	lift force magnitude, N
$\mathbf{L}$	=	aerodynamic lift force vector, N
L'	=	calculated lift magnitude, inclusive of errors, N
$\boldsymbol{l}$	=	aerodynamic lift force unit vector, N
M_K	=	lumped mass of kite and bridles, kg
$\mathbf{N}$	=	Net force vector acting on the kite, kg
n	=	exponent dependent on atmospheric or surface conditions
$\mathbf{R}$	=	kite position vector, m
R	=	kite position vector magnitude (line length, m)
Re	=	Reynolds number (Uc_k/ν)
$\mathbf{r}$	=	kite position unit vector, m
$\mathbf{T}$	=	line tension vector, N
$\mathbf{U}$	=	onset velocity vector, ms^{-1}
U	=	onset velocity magnitude, ms^{-1}
$\mathbf{u}$	=	onset velocity unit vector, ms^{-1}
V_A	=	apparent wind velocity magnitude at the kite when static, ms^{-1}
$\mathbf{V_A}$	=	apparent wind velocity vector at the static when static, ms^{-1}
V_K	=	kite velocity vector magnitude, ms^{-1}
$\mathbf{V_K}$	=	kite velocity vector, ms^{-1}
V_T	=	true wind velocity, ms^{-1}
$V_{T_{\text{ref}}}$	=	reference velocity at altitude Z_{ref}, ms^{-1}
X, Y, Z	=	global Cartesian wind axis system
x, y, z	=	Cartesian position coordinates, m
α	=	angle of attack, deg
α_e	=	effective angle of attack, deg
α_k	=	built-in kite angle of attack, deg
α_t	=	tangent angle of attack, deg
β	=	onset angle in horizontal plane
γ	=	onset angle at kite in vertical plane, deg
δ	=	velocity error, ms^{-1}
ε	=	drag angle, deg
θ	=	elevation angle, deg
μ	=	substitution variable, $\mu = \frac{1}{2}\rho_a A_K C_L \sec\varepsilon$
ρ_a	=	density of air (1.19 kgm^{-3} at 20°, 1 bar)
υ	=	kinematic viscosity of air taken to be 1.52×10^{-5}, m^2s^{-1}
ϕ	=	azimuth angle, deg
Ψ	=	yaw angle of gimbaled kite attachment arm, deg
Ω	=	pitch angle of gimbaled kite attachment arm, deg
ω	=	angular velocity, rad s^{-1}

Received 3 April 2009; accepted for publication 9 September 2009.

*Research Engineer, Fluid Structure Interactions Research Group; Gmd204@soton.ac.uk.

†Senior Lecturer, Fluid Structure Interactions Research Group; dominic@soton.ac.uk.

‡Head of Research, Fluid Structure Interactions Research Group; R.A.Shenoi@soton.ac.uk.

I. Introduction

KITES have hitherto been the subject of a low volume of research for propulsion and power production, but are now receiving growing interest in view of these commercial applications. Their use for ship propulsion was first documented in 1903 when S.F. Cody was reported to have crossed the English Channel under kite power [1]. Significant advances now make large-scale application feasible. These developments were driven initially by the sport of kite surfing, and more recently by the application of large towing kites to ships to reduce fuel consumption and for the wind- assisted generation of electrical power [2–4]. The use of kites for commercial shipping propulsion yields financial savings for the ship operators and minimizes the harmful effect that shipping has on the environment.

An understanding of the dynamics that affect kite motion and the resulting forces can facilitate the design and optimization of kite propulsion systems. This paper investigates theoretical methods for modeling the expected towing line tension for kites when flown in the two distinct modes of kite flight, static and dynamic.

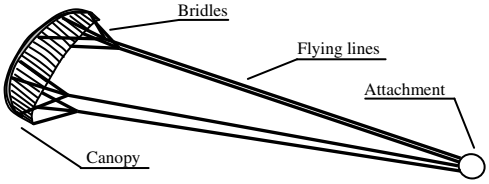

Fig. 1 Parafoil kite.

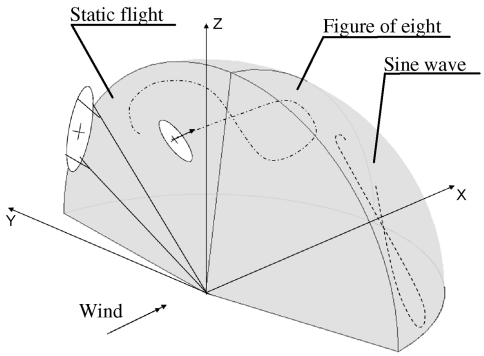

Fig. 2 FE and example flying maneuvers.

The parafoil-type kite has emerged as most common for traction applications (see Fig. 1). The flying lines can be used to maintain a static position relative to the attachment or to maneuver the kite around a continuous path. Examples of dynamic maneuvers are the sine wave and the figure of eight shown in Fig. 2. The sine wave employs a vertical up and down motion as far away from the downwind direction as possible to maximize upwind sailing performance; when moving, this motion inscribes a path that resembles a sine wave when viewed in fixed earth coordinates. The figure of eight maintains a predominantly downwind kite position to maximize downwind sailing performance. Circular flying motions are typically prohibited due to undesirable twisting of the flying lines.

Significant force amplification arises for dynamic kite flight as a result of the increased onset velocity due to the motion of the kite. The maximum onset velocity is found as the wind velocity at the static kite multiplied by a factor approximately equal to L/D [5]. This occurs when the kite is flown directly downwind. Thus, with the aerodynamic force increasing with the square of the onset velocity for a typical value of $L/D = 5$, a maximum lift force in the order of 25 times that of the static kite or sail is achievable.

Because a large component of the kite's onset velocity is created in the crosswind direction due to the motion of the kite itself, the kite is the only wind propulsion device that is able to produce a downwind drive force that is composed predominantly of lift rather than drag.

Wellicome [6] compares suitable candidates for ship propulsion including soft sails, high-lift aerofoils (with lift coefficient, $C_L \sim 3$), high-lift Flettner rotors, and kites. In terms of the drive force achievable per unit area, kites were shown to outperform almost all other viable wind propulsion concepts. When a lift coefficient of 0.65 was used, the kite was only outperformed by the high-lift aerofoil close to the wind but was shown to be the only device capable of generating large drive-force coefficients downwind.

The kite has significant practical advantages that make its commercial application attractive. Because the line tension acts through its tether at deck level, the heeling moment arm (between the center of hydrodynamic and aerodynamic centers of effort) is reduced greatly compared with other conventional sailing rigs. Further, because the towing kite may be mounted at the bow,[§] and does not require a large support structure such as a mast, they can be retrofitted without affecting the existing deck layout or operation. Additional performance benefits can be realized by raising the propulsive kites higher in the atmospheric boundary layer enabling exploitation of stronger winds at altitude. However, for propulsion this must be traded with the reduced forward drive-force component that arises with increased elevation angle.

Kites also lend themselves to other applications. Williams [7] models a tethered kite system for the generation of electrical power. The flying line that is paid out rotates a drum as it unwinds. The kite system is modeled as a collection of point masses connected by inelastic rods. Lagrange's equations are used to define the system through energy consideration. In the computer simulation, a feedback controller is implemented to follow a reference trajectory. A similar approach is adopted to assess the performance and optimize the flying motions of an alternative kite-driven vertical axis generator [8] and also for towing a vehicle in a crosswind direction [9]. Further work by Williams et al. [10] addresses a tracking controller that is numerically implemented to maneuver a kite in the presence of gusts. The angle of attack is controlled to maintain a desired tether tension and the tether length is varied.

Williams et al. [11] consider the actuated steering control of an experimental test kite, first using drag flaps and then via manipulation of the kite line attachment along tracks at the tip of the kite. Preliminary work is conducted to model the flexibility of the kite canopy itself by considering it to be two jointed flat plates [12].

Ockels [3] gives consideration to the power production and economic issues associated with a particular design concept for electricity generation. The concept makes use of several kites on a continuous looped flying line.

Research into applications of new materials and kite construction methods is also ongoing. Breukels and Ockels [13] investigate the application of composites as well as optimizing bridle configurations from a structural perspective for the development of an inflatable kite plane. Jackson [14] looks specifically at improving kite performance by optimizing the shape and twist distribution using lifting line theory applied to a tensioned kite canopy.

Because kites do not readily lend themselves to testing in a wind tunnel due to prohibitively long flying lines and stability issues at small scale, testing can be best achieved by conducting full-scale tests. Alexander and Stevenson [15] developed a test rig for kite performance measurement that was mounted on the roof of a car for towing tests in the natural wind. In addition, work is also conducted that examines the force balance for a kite. It was shown how the static flying position can be predicted from its aerodynamic properties [16]. Stevenson et al. [17] and Stevenson and Alexander [18] developed a testing method for establishing kite L/D by flying the kite in a complete horizontal circle. These experimental studies focused on static flight performance rather than on the characteristics of dynamic flight.

Wellicome and Wilkinson [19] conducted a purely theoretical study of kite maneuvering theory to determine the time-averaged force components when undergoing various flying patterns. It was shown that the onset velocity at the maneuvered kite can be approximated as a function of its spherical coordinates as

$$U = V_A \frac{\cos\theta\cos\phi}{\sin\varepsilon} \tag{1}$$

An assumption is made here that the kite and the lines are weightless; hence this is referred to in the present study as the zero mass model. Under the assumption of zero mass, the line tension vector is equal and opposite to the aerodynamic force vector. Additionally, the drag on the flying line is considered negligible such that it forms a straight line between the tether and the kite.

Naaijen et al. [20] developed a dynamic kite force model for investigating the performance of ships propelled with kites. Under various operating conditions the potential fuel savings were determined. The dynamic model used the kite position vector, the true wind, and the kite velocity to obtain the onset flow. Then, given the performance in terms of L/D, the kite velocity is determined numerically as that which makes the aerodynamic force vector parallel with the flying lines. The magnitude and direction of the aerodynamic force vector can then be determined. As for the zero mass models, this approach implies instantaneous equilibrium.

[§]Pamphlet "Skysails Technological information" available from www.skysails.com.

Bryant and Brown [21] considered the stability characteristics using theory borrowed from conventional aerodynamics. After World War II, attempts were made to develop an early high-performance kite of glider-type design, but it was commented that ensuring stability became increasingly difficult for kites with higher performance in terms of L/D and "the development of a satisfactory kite of high efficiency was reckoned to be so formidable a problem that interest in the subject inevitably declined."

Existing dynamic kite models may be distinguished as using two distinct principles, those which are based upon equilibrium between kite forces and line tension [20,22] and those which employ Newton's equations of motion [8,23–27]. To date, a dynamic model for predicting time histories of line tension during dynamic flight has not been validated experimentally.

The aim of the current paper is to establish whether or not the assumption of zero mass and thus immediate equilibrium can be used effectively to predict kite onset velocity and resulting line tension. This is achieved by comparing predictions using the zero mass model [28] with experimental results. This necessitates the recording of time histories during dynamic kite flight, which has required the development of new testing methods. It is also intended to identify the extent to which the effects of kite mass are significant. This is determined by comparing predictions using the zero mass model with those obtained using a newly developed method based on the equations of motion for a kite and including terms of mass.

II. Mathematical Models

In this section, the zero mass and the lumped mass models are explicitly presented. General aerodynamic concepts pertinent to the current study together with introductory concepts in kite dynamics are also described herein.

A. General

In conventional aerodynamics, the vectors **L** and **D** are the orthogonal components of **F**, perpendicular and parallel to **U**. The magnitudes L and D are given and expressed in their nondimensional forms by

$$L = \frac{1}{2}\rho A U^2 C_L \quad \text{or} \quad C_L = \frac{L}{0.5\rho U^2 A} \tag{2}$$

and

$$D = \frac{1}{2}\rho A U^2 C_D \quad \text{or} \quad C_D = \frac{D}{0.5\rho U^2 A} \tag{3}$$

The magnitude of the line tension or equivalently, the aerodynamic force vector is given and expressed in their nondimensional forms by

$$T^2 = F^2 = D^2 + L^2 \quad \text{or} \quad C_F = \frac{F}{0.5\rho U^2 A} \tag{4}$$

The angle subtended between the lift vector and the aerodynamic force vector is the drag angle ε. When zero mass, or equivalently, instantaneous equilibrium is assumed, **F** and **T** are equal and opposite, although when mass is considered, weight and the force due to acceleration must be included in the balance of forces. The importance of neglecting these terms due to kite mass is considered through comparison of two alternative theories presented in Secs. II.C and II.D.

Figure 3 shows the balance of forces neglecting terms of mass. Through vector algebra, $\mathbf{T} + \mathbf{L} = -\mathbf{D}$, such that the lift and the line tension together produce a force that tends to induce kite motion forward. The drag force opposes this and must be overcome if a positive net force, forward, is to generate kite speed during dynamic flight. The L/D ratio, or equivalently the drag angle, is therefore a measure of the kite performance in terms of its ability to generate kite speed.

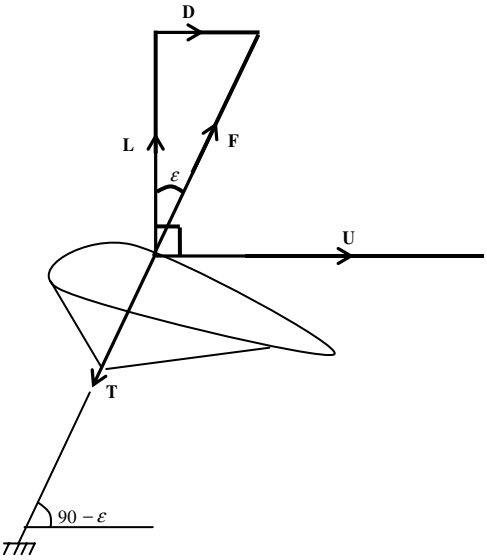

Fig. 3 Forces acting on the statically flown kite under the assumption of zero mass.

From geometric considerations in Fig. 3, the drag angle and the L/D ratio are related by

$$\varepsilon = \tan^{-1}\left(\frac{1}{L/D}\right) \tag{5}$$

which together with Eq. (1) demonstrates that higher L/D results in higher onset velocity, thus improving the lift generating capability.

Figure 3 also illustrates how the kite performance in terms of its drag angle, and thus L/D, can be measured experimentally. The drag angle is obtained by direct measurement of the angle $90 - \varepsilon$ when flown statically in the vertical position. L/D is then obtained using Eq. (5). This principle is used to obtain the kite performance characteristics during experimental validation.

B. Wind Model

In natural conditions the apparent wind speed at a static kite can fluctuate significantly. Wind statistics can be used to predict the variation in kite performance. At heights of up to 30 m the standard deviation in the wind speed is found to be 10–25% of the mean and the variation in the wind direction can be 10–15 deg either side of the mean [29].

In addition to the spatial variability of the wind, vertical variability is present in the atmospheric boundary layer in which the wind velocity is slowed by viscous effects. In the lower atmosphere, the wind may be approximated by a power law that is given by [30]

$$V_T = V_{T_{\text{ref}}}\left(\frac{Z}{Z_{\text{ref}}}\right)^n \tag{6}$$

A typical value for the exponent is $n = 1/7$.

C. Zero Mass Model

With a view to providing a simplified model for kite maneuvering, Wellicome and Wilkinson [31] formulated the zero mass analysis. The simplifying assumptions are that 1) the kite maneuvers on a spherical surface of constant radius, and 2) the kite mass, the cable mass, and the cable drag are all negligible.

Because gravitational and inertial forces are neglected and the flying line is assumed to be straight, the aerodynamic kite force and the line tension reach equilibrium instantaneously so that they are colinear with the flying line at all points in space for all time.

The onset velocity can be expressed as

$$\mathbf{U} = U\mathbf{u} = V\mathbf{v} - R\dot{\mathbf{r}} \tag{7}$$

The aerodynamic force magnitude is given by

$$F = L \sec \varepsilon = \frac{1}{2}\rho_a A_k U^2 C_L \sec \varepsilon = \mu U^2 \tag{8}$$

The lift force magnitude is given by

$$L = \frac{1}{2}\rho_a A_K U^2 C_L = \mu U^2 \cos \varepsilon \tag{9}$$

The drag force magnitude is given by

$$D = \frac{1}{2}\rho_a A_K U^2 C_D = \mu U^2 \sin \varepsilon \tag{10}$$

By vector addition

$$\mathbf{F} = F\mathbf{r} = L\mathbf{l} + D\mathbf{u} \tag{11}$$

where $\mathbf{l}$ is a unit vector perpendicular to $\mathbf{u}$ so that $\mathbf{l} \bullet \mathbf{u} = 0$. Substituting for F, L, and D

$$\mu U^2 \mathbf{r} = \mu U^2 \cos \varepsilon \mathbf{l} + \mu U^2 \sin \varepsilon \mathbf{u} \tag{12}$$

or

$$\mathbf{r} = \mathbf{l} \cos \varepsilon + \mathbf{u} \sin \varepsilon \tag{13}$$

Taking the scalar product with onset unit direction $\mathbf{u}$

$$\mathbf{r} \bullet \mathbf{u} = \mathbf{l} \bullet \mathbf{u} \cos \varepsilon + \mathbf{u} \bullet \mathbf{u} \sin \varepsilon \qquad \therefore \mathbf{r} \bullet \mathbf{u} = \sin \varepsilon \tag{14}$$

By taking scalar products with the position unit vector Eq. (7) becomes

$$U\mathbf{u} \bullet \mathbf{r} = U \sin \varepsilon = V\mathbf{v} \bullet \mathbf{r} - R\dot{\mathbf{r}} \bullet \mathbf{r} \tag{15}$$

Because motion is confined to the surface of a sphere, the kite velocity is tangential to its surface such that $\mathbf{r} \bullet \dot{\mathbf{r}} = 0$. It follows that

$$U = \frac{V\mathbf{v} \bullet \mathbf{r}}{\sin \varepsilon} \tag{16}$$

A Cartesian right-handed system is chosen with the wind parallel to the X axis. The position angles of the vectors $\mathbf{R}$ and $\mathbf{U}$ are as shown in Fig. 4. The position angles of $\mathbf{U}$are β and γ.

With reference to Fig. 4, the unit vectors $\mathbf{v}$, $\mathbf{r}$, and $\mathbf{u}$ are expressed in terms of their position angles as

$$\mathbf{v} = \{1, 0, 0\} \tag{17}$$

$$\mathbf{r} = \{\cos\theta\cos\phi, \cos\theta\sin\phi, \sin\theta\} \tag{18}$$

$$\mathbf{u} = \{\cos\gamma\cos\beta, \cos\gamma\sin\beta, \sin\gamma\} \tag{19}$$

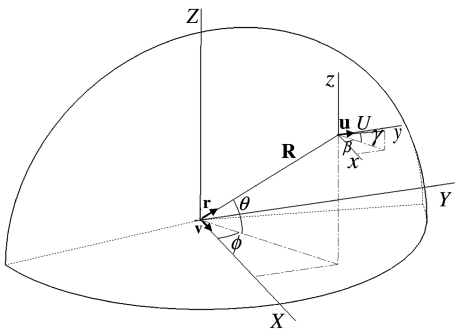

Fig. 4 FE showing position angles for the kite and the onset velocity U.

and $\dot{\mathbf{r}}$ is then obtained by differentiation of $\mathbf{r}$ as

$$\dot{\mathbf{r}} = \{-\cos\theta\sin\phi\dot{\phi} - \sin\theta\cos\phi\dot{\theta}, \cos\theta\cos\phi\dot{\phi} - \sin\theta\sin\phi\dot{\theta}, \cos\theta\dot{\theta}\} \tag{20}$$

Substituting into Eq. (7) yields

$$U\{\cos\gamma\cos\beta, \cos\gamma\sin\beta, \sin\gamma\} = \{V + R\cos\theta\sin\phi\dot{\phi} + R\sin\theta\cos\phi\dot{\theta}, R\sin\theta\sin\phi\dot{\theta} - R\cos\theta\cos\phi\dot{\phi}, -R\cos\theta\dot{\theta}\} \tag{21}$$

Because $\mathbf{r} \bullet \mathbf{u} = \cos\theta\cos\phi$, Eq. (16) can be expressed as

$$U = V_A \frac{\cos\theta\cos\phi}{\sin\varepsilon} \tag{22}$$

which is Eq. (1) in Sec. I.

D. Two-Dimensional Lumped Mass Model

The lumped mass model was developed for comparison to the zero mass model to establish the effect of neglecting terms of mass. This model is based on the equations of motion for a kite and considers the kite as a point mass, lumped at the end of a flying line. The flying line is assumed to be straight, weightless, and inextensible. The net forces acting on the kite are calculated for a known set of aerodynamic characteristics in terms of C_L and L/D for different α, kite velocity, and position, and apparent wind at the kite as if the kite is static relative to its tether. From these, an instantaneous acceleration is obtained. This acceleration is assumed to remain constant during a small time step. The resulting velocity and displacement at the end of the time step are calculated. The process is continued until kite motion along a predefined flight path is completed.

This process differs from the zero mass model as it determines the outputs as a function of time, rather than solely a function of position. The forces acting in the lumped mass model are shown in Fig. 5a. The flight envelope (FE), which determines the limiting positions of the kite during practical flight, is also shown in the figure.

The kite velocity is

$$\mathbf{V_k} = R\dot{\mathbf{r}} \tag{23}$$

Unit direction $\mathbf{r}$ is expressed as

$$\mathbf{r} = \begin{pmatrix} R\cos\theta \\ R\sin\theta \end{pmatrix} \tag{24}$$

The onset velocity is determined as for the zero mass model using Eq. (25)

$$\mathbf{U} = \mathbf{U_A} - \mathbf{V_K} \tag{25}$$

The components of the onset velocity $\mathbf{U}$ are shown in Fig. 5b. The effective angle of attack at which the kite operates is the angle between the chord line and the onset velocity. The kite has a built-in angle of attack relative to the tangent to the FE. This is a known geometric constant. These angles are shown in Fig. 5c.

The angle of attack relative to the tangent line ($\alpha_t = \alpha_e + \alpha_K$) is given by

$$\mathbf{U} \bullet \mathbf{V_K} = -UV_K \cos(\alpha_e + \alpha_K) \tag{26}$$

$$\therefore (\alpha_e + \alpha_k) = \cos^{-1}\left(-\frac{\mathbf{U} \bullet \mathbf{V_K}}{UV_K}\right) \tag{27}$$

Hence, α_e may be obtained.

The lift and drag coefficients C_L and C_D are obtained as

$$C_L = f(\alpha_e, Re) \quad \text{and} \quad C_D = g(\alpha_e, Re) \tag{28}$$

where f and g are properties of a given kite geometry and may, for example, be obtained from wind-tunnel experiments.

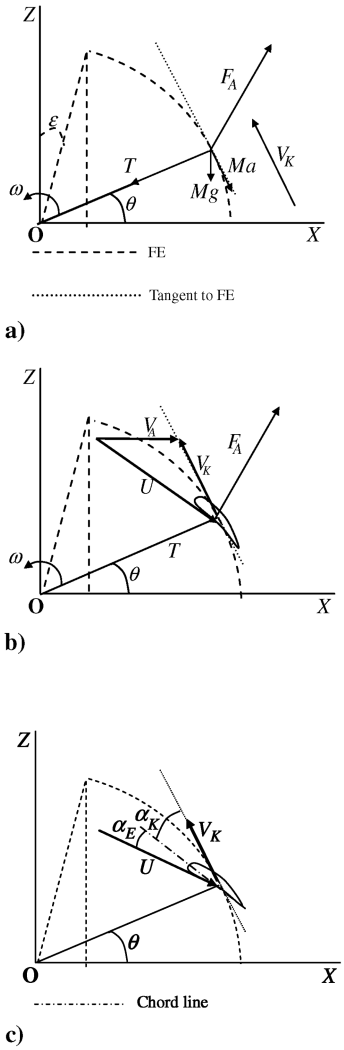

Fig. 5 a) Lumped mass model for motion in the vertical plane $\phi = 0$, b) relationship between U, V_A , and V_K, and c) relationship between α_t, α_e, and α_k.

The lift and drag force magnitudes are

$$L = qC_L A_K \quad \text{and} \quad D = qC_D A_K \tag{29}$$

where $q = \frac{1}{2}\rho U^2$.

The weight of the kite is

$$\mathbf{W} = M_K \mathbf{g} \tag{30}$$

The net force acting on the kite is given by

$$\mathbf{N} = \mathbf{L} + \mathbf{D} + \mathbf{W} \tag{31}$$

The kite line is incapable of supporting any bending moment or shear force. It is assumed to have zero weight and drag such that it adopts a straight line form. Therefore, line tension is equal and opposite to the radial components of the net force. The circumferential components of the net force lead to the acceleration of the kite.

The line tension is given by the projection of the net force onto the radial direction as

$$\mathbf{T} = T\mathbf{r} = (\mathbf{N} \bullet \mathbf{r})\mathbf{r} \tag{32}$$

The circumferential component of net force has a unit direction vector at right angles to the position vector given by

$$\mathbf{c} = \begin{pmatrix} 0 & 1 \\ -1 & 0 \end{pmatrix} \mathbf{r} \tag{33}$$

The magnitude of the circumferential component is equal to the projection of the net force onto the circumferential direction, given by

$$C = \mathbf{N} \bullet \mathbf{c} \tag{34}$$

The circumferential force is thus

$$\mathbf{C} = C\mathbf{c} \tag{35}$$

The linear acceleration is obtained using Newton's second law of motion as

$$\mathbf{a}_\mathbf{K} = \frac{\mathbf{C}}{M_K} \tag{36}$$

The angular acceleration is

$$\dot{\omega} = \frac{C}{M_K R} \tag{37}$$

The new angular velocity after time step Δt is obtained using a forward difference Euler integration scheme

$$\omega_{k(n)} = \omega_{K(n-1)} + \dot{\omega}_{K(n-1)} \Delta t \tag{38}$$

The new linear kite velocity is

$$V_K = \omega_K R \tag{39}$$

The new elevation is

$$\theta_{(n)} = \theta_{(n-1)} + \omega_{K(n-1)} \Delta t \tag{40}$$

The preceding formulation is sufficient to define the kite performance for a given instant in time along a two-dimensional flight path.

III. Implementation of Theoretical Models

A. Zero Mass Model Implementation

Prediction of kite onset velocity using the zero mass model was calculated using Eqs. (7–22). Lift, drag, and hence line tension were then obtained using Eqs. (2–4). The calculation required the provision of a series of instantaneous kite position angles around a prescribed maneuver. For a purely theoretical study, the flight paths could have been selected arbitrarily. In the present study, the process was implemented using real recorded kite flight paths so that the experimental results could be directly compared.

B. Lumped Mass Model Implementation

A flow chart describing the implementation of the lumped mass model is shown in Fig. 6. It follows Eqs. (23–40). This process was implemented for a simple two-dimensional maneuver using different values for the kite mass, thus allowing the implications of the zero mass assumption to be assessed through direct comparison of the two models.

In practical flight, a hot launch maneuver satisfies the requirements for flight in two dimensions. The kite is positioned directly downwind facing upward and is flown directly toward the zenith position. This simple maneuver may also be replicated experimentally with relative ease. The two-dimensional lumped mass model can also be used to assess the performance of kite flight in a downward direction by modifying the initial conditions for which the model is run. The future development of a three-dimensional lumped mass model to three dimensions will allow the investigation of maneuvers such as the figure of eight, commonly used in practice.

The built-in angle of attack in Fig. 5 was obtained photographically for the current test kite by taking a side view of the undeformed kite when inflated by the natural wind. It was determined by measuring the angle between the tensioned flying lines and the chord using MATLAB® [32] plotting tools. The center of the air inlet and a point on the trailing edge were used as reference points for the chord line.

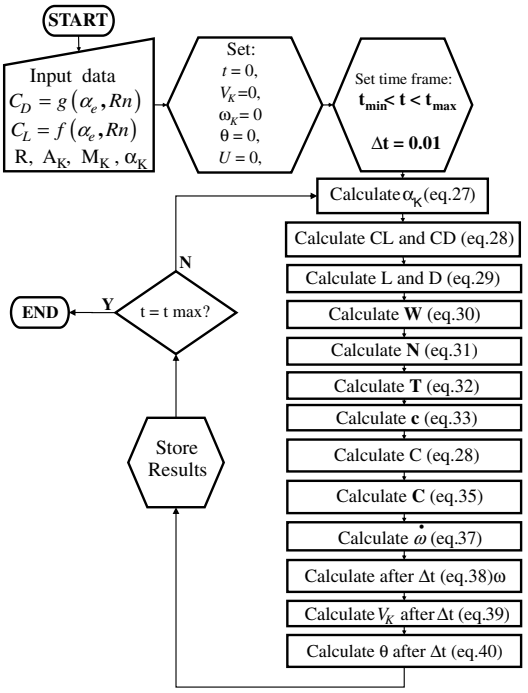

Fig. 6 Flow chart for lumped mass model implementation.

Flight performance characteristics of the experimental test kite (Flexifoil Blade III, 3 m^2) were required, as described by Eq. (28) for C_L, C_D, and L/D to be obtained for any α_e by means of a look-up table. The compliant nature of foil kites makes testing at different angles of attack in a wind tunnel problematic; thus, in the absence of such data for the test kite, an approximation was derived using experimental results [33] for a NACA 4415 foil section. This foil was selected to closely match that of the test kite and the experimental results satisfied the unusual requirement that the performance data be known for very large effective angles of attack, up to deep stall. The data were presented for an aspect ratio of 6; therefore, a correction was made to adjust the data for the experimental test kite with an aspect ratio of 4.86 using Eqs. (41) and (42) [34]

$$C'_D = C_D + \frac{C_L^2}{\pi}\left(\frac{1}{AR'} - \frac{1}{AR}\right) \tag{41}$$

$$\alpha' = \alpha + \frac{C_L}{\pi}\left(\frac{1}{AR'} - \frac{1}{AR}\right) \tag{42}$$

C'_D and α' correspond, respectively, to the drag coefficient and angle of attack (radians) of a wing of aspect ratio AR'.

A further correction to the NACA 4415 performance data was made to account for line and bridle drag. It was assumed that during dynamic flight, the onset velocity remained approximately normal to the bridles and lines, such that the drag can be expressed as

$$D_{BL} = \frac{1}{2}\rho U^2 A_{BL} C_{D_{BL}} \tag{43}$$

The drag coefficient of a cylinder of infinite aspect ratio is taken to be 1.2 [35], appropriate for $10^2 < Re < 10^3$ for practical onset velocities. The combined drag coefficient for the NACA 4415 foil together with the lines and bridle was approximated by Eq. (44)

$$D_{\text{Tot}} = D_{BL} + D_K = \frac{1}{2}\rho U^2 \cdot A_{BL} \cdot C_{D_{BL}} + \frac{1}{2}\rho U^2 \cdot A_K \cdot C_{D_K}$$

$$= \frac{1}{2}\rho U^2 (A_{BL} \cdot C_{D_{BL}} + A_K \cdot C_{D_K})$$

$$C_{D_{\text{Mod}}} = \frac{(A_{BL} \cdot C_{D_{BL}} + A_K \cdot C_{D_K})}{A_K} \tag{44}$$

The modifications described by Eqs. (41–44) were applied to the experimental aerofoil data [33] to derive the assumed kite performance characteristics as shown in Table 1. These data were used to implement the lumped mass model for comparison to the zero mass model and experimental results.

IV. Experimental Methods

A. Apparatus

A system capable of measuring time histories of the full-scale kite force vector during flight was developed, shown in Fig. 7 in a schematic form.

The angular displacement transducers (model spectrol 157 manufactured by Vishay) were used to measure the two Euler angles pitch and yaw. These angles were sufficient to define the kite line tension vector orientation and the approximate Cartesian kite position coordinates using a known line length.

The load cell (model serial number 17605762, manufactured by LCM Ltd. systems) was used to obtain the line tension. It has a rated full range of 98100 N with specified accuracy ±0.03%. The transducers were configured on a gimbaled flying arm as shown in Fig. 8.

The apparatus was mounted on a welded support for the instrumented gimbals as shown in Fig. 9. This support defined the frame of reference in which the apparent wind velocity, the kites' relative wind velocity and kite force vector were established.

The wind velocity transducer (ST40 Rota vector type anemometer, manufactured by Raymarine) was mounted on a 6 m aluminum mast to minimize the influence of disturbances caused by ground obstructions. It was attached to the trailer via a detachable support and stays were used to improve fixation. The linearity of the anemometer was 2%, as established using the wind tunnel. The wind velocity signal was damped using a 3 s average period. The data acquisition system comprised a signal conditioning amplifier, an analog to digital converter (AD card), and a laptop computer, together with data acquisition program Turbo AD [36]. A schematic diagram for the configuration of the acquisition system is shown in Fig. 10. The amplifier (model Modular 600 manufactured by RDP Electronics Ltd.) has two dual channel subunits with model numbers RDP-611 and RDP-621. The inverter (model Handy Mains 200 watt inverter) was used to convert the car battery voltage from 12 V to the 240 V required by the amplifier and the computer.

B. Calibration

The load cell and the potentiometers were each calibrated independently with the intention of configuring the system so that the best resolution and hence best accuracy could be obtained over the expected range of angles and loads induced by the kite. The calibration procedure, which is outlined in Appendix A, details in turn the methods used to calibrate the load cell and the potentiometers.

Table 1 Assumed kite performance characteristics

α_e/ deg	C_D	C_L	L/D	ε/ deg
−5	0.051	−0.001	−0.358	10.2
0	0.067	0.337	4.864	14.3
5	0.086	0.692	8.015	7.2
10	0.117	0.939	7.991	7.1
15	0.158	1.137	7.292	7.9
20	0.231	1.147	5.132	11.6
25	0.341	0.893	2.746	21.3
30	0.497	0.789	1.614	32.2
35	0.611	0.770	1.263	38.4
40	0.712	0.735	1.035	44.1
45	0.812	0.701	0.867	49.1
50	0.914	0.686	0.752	53.1
55	1.010	0.635	0.631	57.8
60	1.102	0.552	0.501	63.4
65	1.176	0.455	0.388	68.9
70	1.244	0.349	0.281	74.3
75	1.295	0.223	0.173	80.2
80	1.333	0.080	0.061	86.6

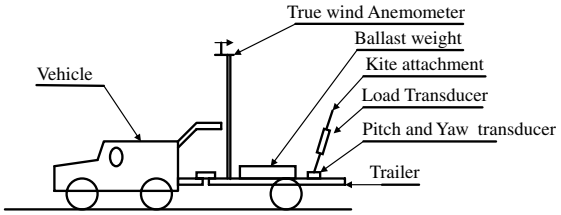

Fig. 7 Schematic layout of kite testing apparatus.

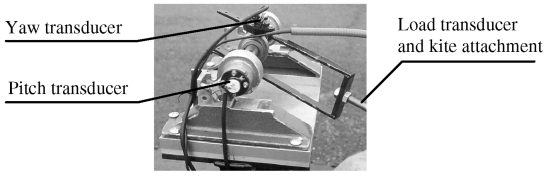

Fig. 8 Gimbaled angular displacement transducers, load transducer, and kite attachment.

Fig. 9 The dynamometer and the attached kite.

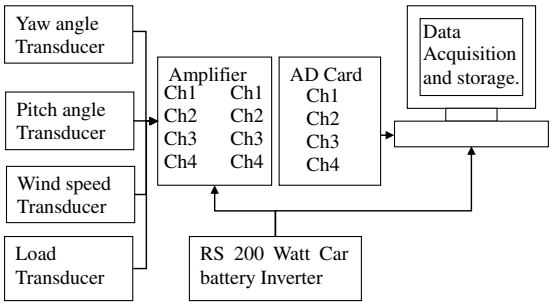

Fig. 10 Schematic view of data acquisition system.

Statistical quantities that describe the accuracy of the complete data acquisition system are also given in Appendix A.

C. Testing

The apparatus was aligned to face downwind. The kite flier was situated on the testing platform behind the kite. The test kite was a 3 m^2 Flexifoil Blade III. The particulars for the kite were measured and are shown in Table 2.

1. *Defining the Flight Envelope*

The spatial orientation of the FE was established before each test to orientate the axis system for analysis. The kite was set in its starboard-most equilibrium position, with one wing tip close to the ground for 10 s. This enabled a point on the starboard-most edge of the FE to be defined using a time-averaged result. The kite was then moved slowly to the zenith position and the port-most position, again pausing for 10 s. In the analysis of flight trajectories, the downwind axis (X axis) was taken to be the bisector of these vertices because the kite makes the same angle to the wind on both sides of the FE.

Table 2 Kite particulars for Flexifoil Blade III 3 m

Span	3.8 m
Area	2.984 m^2
AR	4.86
Line length (four lines)	28.0 m (four lines)
Bridle configuration total length	41.6 m
Bridle and flying line diameter	1 mm

2. *Static Kite Performance Characteristics*

In very light airs, the FE definition and the static performance tests were conducted using artificially created winds. This was achieved by towing the test rig to maintain an apparent wind of 15 kt.

Both the line tension and the angle $90 - \varepsilon$ were measured during static flight. A time-averaged static measurement was taken to minimize the effect of small disturbances in very light airs. With reference to Fig. 3, these were used to infer the aerodynamic force vector and thus obtain **L** and **D**. The onset wind velocity **U** was obtained directly from the anemometer. C_L, C_D, and L/D were then calculated using Eqs. (1) and (2). The resulting performance parameters are given in Table 3, together with the 95% and 99% confidence intervals.

3. *Dynamic Testing*

Dynamic tests were done to evaluate the force amplification achievable by flying the kite dynamically within the FE. These tests enabled experimental comparison to both the zero mass and the lumped mass models of Sec. II. For the lumped mass model, the comparison was limited to the two-dimensional hot launch maneuvers, However, for the zero mass model comparison was also made for dynamic three-dimensional figure of eight maneuvers, typical of ship propulsion.

The flight tests were conducted in approximately 7 m/s natural wind. Having spatially defined the FE by pausing at the three vertices, a figure of eight motion was flown using approximately 70% of the horizontal and vertical extent of the window for each complete cycle. The kite was also hot launched from static at ground level, vertically upward to the vertical zenith position. When this launch method was used, the kite was typically stalled prelaunch due to its orientation. Therefore, the hot launch maneuver allows recovery to its natural unstalled velocity to be assessed, as determined by Eq. (22).

Control of the flown kite was achieved manually via steering lines passed through a shackle mounted on the load cell. Care was taken to apply an equal opposing force to the left and right flying lines so the line was fed through the shackle with minimal force, added manually. Although the control forces are not measured, it is noted that they are small compared with the kite-induced loads and thus, no correction is applied to the results. Additionally, the control inputs were only required at the point in each figure of eight in which the direction of turn was reversed because the friction in the system was sufficient to maintain the desired rate of turn.

D. Method of Experimental Analysis

The Euler angles output by the gimbaled potentiometers were converted to Cartesian position coordinates using

$$x = R\cos\Omega\cos\Psi \qquad y = R\sin\Psi \qquad z = R\cos\Omega\sin\Psi \tag{45}$$

Table 3 Statically measured performance characteristics for the test kite (Flexifoil Blade III 3 m)

	ε	L/D	C_F	C_L	C_D
N samples	21	21	21	21	21
Mean	9.55	6.07	0.786	0.776	0.128
Standard deviation	1.48	0.88	0.115	0.116	0.012
95% confidence limit	0.63	0.38	0.049	0.050	0.005
99% confidence limit	0.83	0.50	0.065	0.065	0.006

The required spherical coordinates were obtained assuming a straight line form as

$$\phi = \tan^{-1}\left(\frac{y}{x}\right) \tag{46}$$

$$\theta = \tan^{-1}\left(\frac{z}{\sqrt{x^2 + y^2}}\right) \tag{47}$$

For comparison of the zero mass and the lumped mass models with experiment it was necessary to derive the appropriate quantities from the experimentally measured variables. The experimentally measured onset velocity was derived using Eq. (7), repeated here for convenience

$$\mathbf{U} = U\mathbf{u} = V\mathbf{v} - R\dot{\mathbf{r}}$$

The first term $V\mathbf{v}$ was derived directly from the anemometer. A correction for the atmospheric boundary layer was applied where appropriate using Eq. (6). The unit vector specifying the direction of the wind was taken to be $v = (1 \quad 0 \quad 0)$, coincident with the X axis.

The second term $R\dot{\mathbf{r}}$ was derived by application of Eq. (20) using the experimentally measured values for θ and ϕ. The time derivatives $\dot{\theta}$ and $\dot{\phi}$ were obtained using a first-order backward differencing scheme. The magnitude of the position vector is defined by the measured line length 28.0 m. A 1 s moving average filter was used to smooth U, based on experience.

The predicted zero mass onset velocity for comparison with experiment was obtained using the measured position angles θ and ϕ together with the measured and boundary layer-corrected wind velocity and by application of Eq. (22), which predicts the theoretical onset velocity. The measured line load was determined directly from the load cell. The predicted zero mass line load was determined using the predicted zero mass onset velocity, together with the statically measured performance characteristics C_L, C_D, and C_F with application of Eqs. (2–4).

V. Results and Discussion

A. Static Kite Performance Measurements

Experimentally measured static performance characteristics for the Flexifoil blade III, as described in Sec. IV.C, are shown in Table 3. With 95% confidence limits, $\varepsilon = 9.55 \pm 0.63$, $L/D = 6.07 \pm 0.05$, and $C_L = 0.776$. The in-built angle of attack for the test kite is determined photographically in accordance with the implementation of the lumped mass model of Sec. III.B as $\alpha_K = -9$ deg.

B. Basic Implementation of Zero Mass Theory

Figure 11 shows in polar form how the onset velocity varies for different positions of the kite relative to the wind in the horizontal XY plane and in the vertical XZ plane. The results are predicted using the zero mass theory of Sec. II using a wind speed of 10 m/s. The limiting positions of the kite are indicated by the line of static equilibrium. It is noted that the lift increases with the square of the onset velocity, and the maximum onset velocity is approximately determined as the wind speed multiplied by L/D. Hence for the case shown, where $L/D = 6$, the peak load is in the region of 36 times that of the static kite.

Constant values for ε and hence L/D and C_L have been assumed in accordance with the zero mass theory [37].

C. Comparison of Zero Mass and Lumped Mass Theory with Experiment

Figure 12 shows the experimentally recorded position angles for a hot launch maneuver followed by a figure of eight maneuver.

Figure 13 presents experimentally measured load induced during the hot launch; this is compared with theoretical predictions derived using the zero mass and the lumped mass models. It is seen that the lumped mass model predicts loads that are lower than both the zero mass model and the experiments. This can be explained, at least in part, by differences arising in the L/D and C_L for each model. The zero mass model uses the statically measured performance of Table 3 as an input, whereas the lumped mass model yields L/D and C_L, which vary as an output that is dependent on the assumed kite performance data of Table 1.

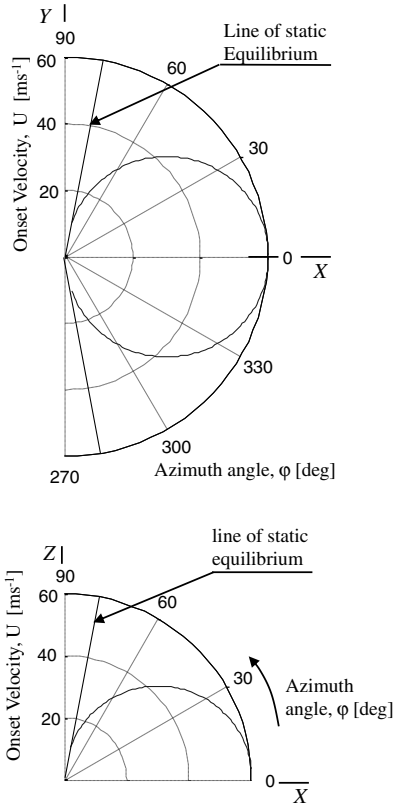

Fig. 11 Onset velocity polar for straight flight maneuvers in two planes: the XY plane (plan view) and the XZ plane (side view). $\varepsilon = 9.55$ deg, $V_A = 10$ ms^{-1}.

D. Comparison of the Zero Mass Theory with the Lumped Mass Theory

Figure 14 compares the loads resulting from the zero mass and the lumped mass models. They are plotted to a base of θ. Direct comparison of the zero mass and lumped mass models requires that each model uses the same kite performance in terms of L/D and C_L. This comparison is made by adopting the static performance values that result from running the lumped mass model until static flight is attained.

Different values for the kite mass are used to obtain line load predictions with the lumped mass model. It can be seen that through setting the mass closer to zero, the results produced by the lumped

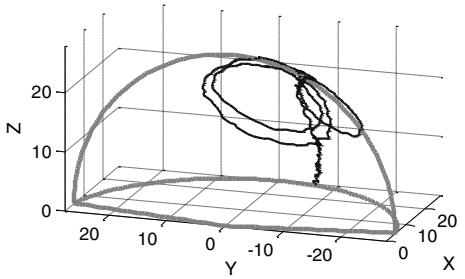

Fig. 12 Experimentally recorded position coordinates for two example basic kite maneuvers, the hot launch, approximating straight flight in the vertical XZ plane followed by the figure of eight maneuver centered downwind.

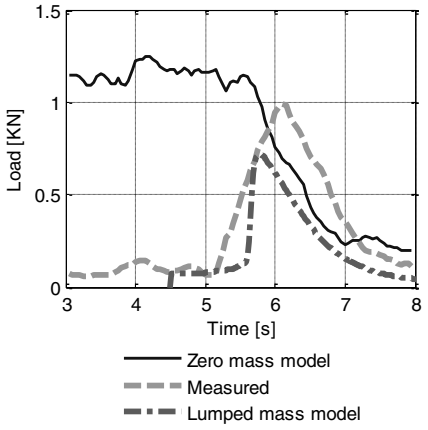

Fig. 13 Comparison of the lumped mass model, zero mass model, and measured load for a hot launch maneuver.

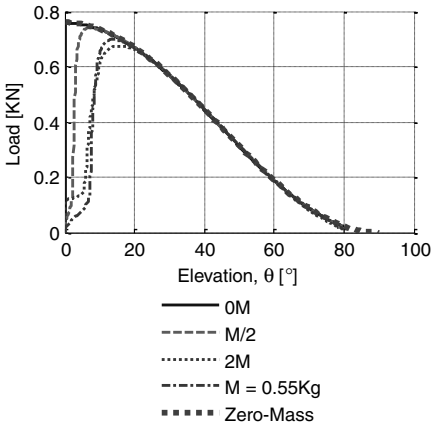

Fig. 14 Comparison of the lumped mass model using different values of kite mass with the zero mass model.

mass model converge toward those of the zero mass model. In the limit where $M = 0$ the results are practically identical.

As for the zero mass model and for the lumped mass model where mass is set close to zero, without the inertial and weight effects of the kite being considered the kite accelerates to its natural velocity instantaneously, as determined by Eq. (22). However, running the lumped mass model with kite mass set to $1/2M$, M, and $2M$ it is seen that inertia of the kite affects performance with increasing significance. The kite takes longer to reach its natural velocity such that the results converge toward the zero mass result at a later point in the maneuver. It is noteworthy that setting the kite mass to $2M$ prevents the model from running unless the kite is initiated with 6 ms^{-1} velocity. This arises because at launch, the kite is deeply stalled and the lift produced in this condition is not sufficient to overcome the weight of the kite. Initiating the kite with a velocity of 6 ms^{-1} brings the kite closer to its unstalled condition. Further, it is seen that the inertia it carries once launched allows it to exceed its natural velocity for the latter part of the launch maneuver, although this effect is small.

It is observed that the zero mass model predicts velocity and hence positive line load until $\theta = 90$ deg, whereas the lumped mass model predicts that the kite comes to rest at $\theta = 80$ deg. In this respect the lumped mass model correctly predicts the limiting position angles of the FE, whereas the zero mass model requires that they be artificially imposed.

E. Analysis of the Lumped Mass Model

Figure 15 presents the time histories of other parameters, which arise in the determination of the predicted line tension using the lumped mass model. Results are shown for actual mass $M = 0.55$ kg (denoted M in the figure) and close to zero mass $M = 0.001$ kg (denoted $0M$ in the figure). They are a) elevation, b) kite velocity, onset velocity, and apparent wind velocity, c) acceleration, d) effective angle of attack, e) drag angle, f) lift-to-drag ratio, g) lift and drag coefficients, and h) lift, drag, and line tension.

In Fig. 15a, the elevation is seen to rise slowly at first before rising quickly at $t \approx 1.5$ s. During this period it is seen in Fig. 15d that the effective angle of attack reduces to $\alpha_e = 20$ deg, and the kite remains fully stalled. This stalled part of the maneuver is characterized by low L/D and low line tension, as seen in Figs. 15f and 15h, respectively. After $t \approx 1.5$ s the kite becomes unstalled and the lift (in Fig. 15h) increases very rapidly, which results in high acceleration of the kite (seen in Fig. 15) until the kite approaches its natural velocity at $t \approx 1.75$ s. Once this is reached, the resulting velocity in Fig. 15b and the line tension in Fig. 15h follow a very similar trend for the cases where $M = 0.55$ and $M = 0$. A slightly higher line tension is achieved in the case where M is close to zero, because the natural velocity is realized for a smaller elevation angle. It can be inferred that the kite will seek this natural velocity, but during some instances when changing conditions occur, it may not be realized and a time delay ensues before it is again achieved. It is noteworthy that the time delay seen here is attributable only to inertial and weight effects, because running the model setting $M = 0$ yields peak line tension at $t = 0$ s.

Poststall, the acceleration in Fig. 15c follows the same pattern for the zero mass case and the standard mass case. This implies that its value is not significantly affected by this small change in weight. The acceleration appears to be determined predominantly as a function of wind velocity rather than being a function of the kite mass. Although the effects of mass are important during stalled flight, in normal flight the terms in the force balance that are affected by mass, that is, the kite weight and inertial forces, quickly become insignificant. This observation could cease to be true if kite design moves toward much larger kites of rigid construction having much greater mass per unit area.

The effective angle of attack in Fig. 15d quickly reduces to $\alpha_e = 0.9$ deg at $t = 2$ s before reaching a minimum 0.25 deg at $t = 3.2$ s and then rising again to 1.9 deg at the point of static equilibrium. The low angle of attack is owed to the dominance of the onset velocity due to kite motion $-V_K$ in Eq. (25). This term contributes only to the component of U that is tangential to the FE. The apparent wind term V_A has a radial component, and therefore tends to increase the effective angle of attack. This becomes increasingly less significant with greater kite velocity V_K.

Interestingly, referring to Fig. 15f, the L/D that corresponds to normal dynamic flight remains well below the maximum that is realized momentarily as the kite accelerates up to its natural velocity. This implies that during dynamic flight, better performance in terms of achievable line tension could be achieved by optimizing the built-in angle of attack.

For the case where the lumped mass is set close to zero, α_e (in Fig. 15c), L/D (in Fig. 15f), and ε (in Fig. 15e) remain constant throughout flight. This implies that the motion of the kite adjusts to achieve its natural angle of attack α_e and L/D, rather than the angle of attack being determined as a result of kite motion and orientation. Hence, in the limit where $M = 0$ kg, constant kite performance in terms of L/D and C_L may be assumed, although when terms of mass (weight and inertial forces) are present and significant, L/D and C_L are affected. This assumption of constant performance becomes less valid with increasing kite mass.

At this stage, it is possible to gain insight into the mechanism that determines the natural velocity. Assuming that L/D is constant, it may be inferred by considering Fig. 5b that increasing the kite velocity vector $\mathbf{V_K}$ has the effect of altering the direction of the onset velocity vector $\mathbf{U}$. This moves the aerodynamic force vector rearward with respect to the flying line. Conversely, slowing the kite moves the aerodynamic force vector forward. For a given position, there is a velocity at which the aerodynamic force vector remains colinear with the flying line. This is the natural velocity, in which the forces balance, not considering terms of mass. In practice, however, the inertial and weight forces that act on the kite modify this ideal force

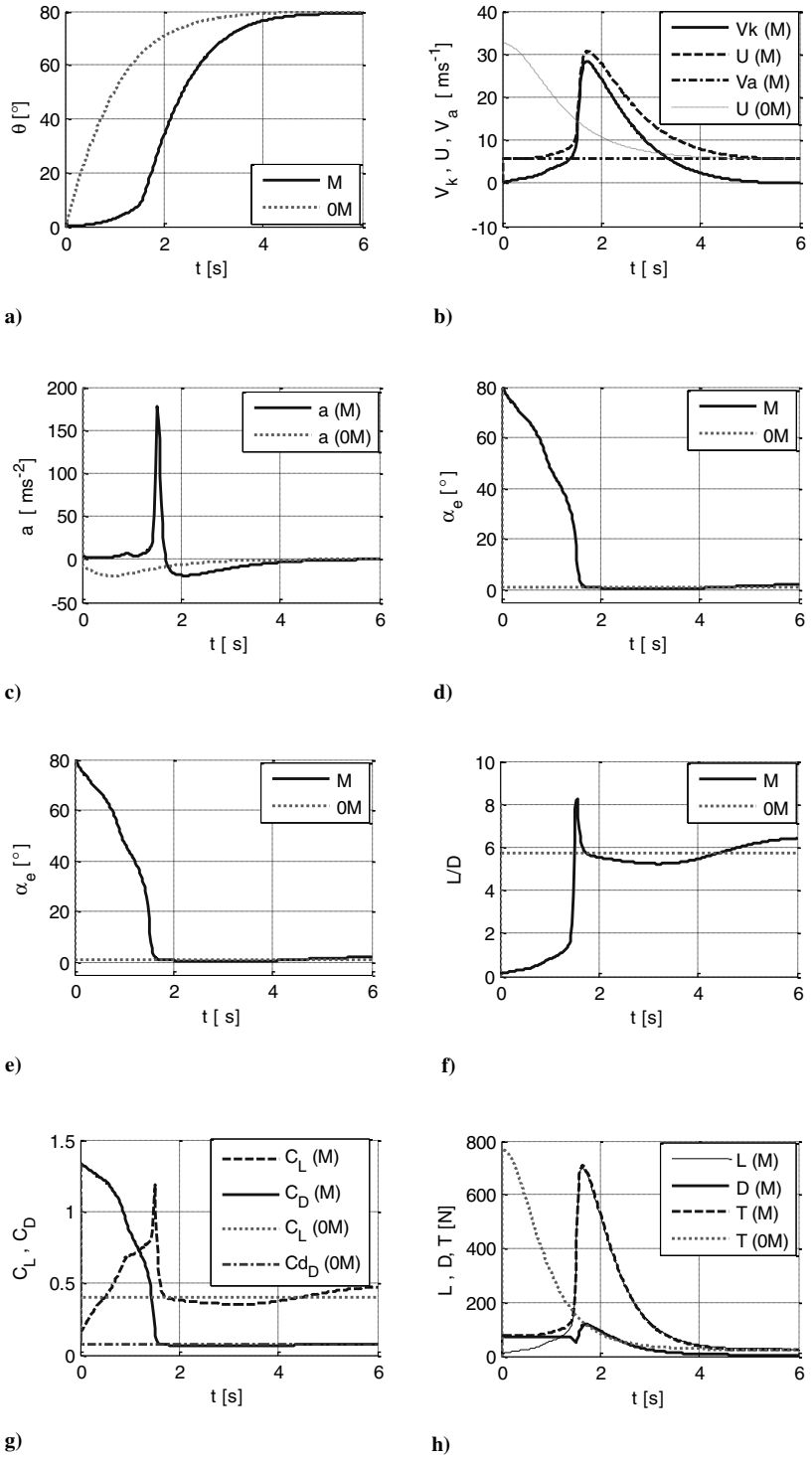

Fig. 15 Time history predictions for hot launch maneuver using the lumped mass model.

balance such that the natural velocity may not be exactly achieved. This observation is apparent in the L/D and C_L traces of Figs. 15f and 15g. It is seen that for the standard mass case, poststall values vary within the range $5.23 < L/D < 6.42$ and $0.35 < C_L < 0.47$.

Decreased velocity arising from the effects of mass during launch is compensated by a corresponding increase in L/D due to the modified angle of attack. An increased velocity appears to be compensated by a reduced L/D. Hence it is not strictly true that L/D remains constant, although the concept of a natural velocity still remains. It is noted that for the example considered, the effects of mass on line tension are very minor. Figure 14 shows that the net result on the line tension is negligible for unstalled flight, and recovery from stall is delayed, or prevented, by increased mass.

F. Analysis of Experimental Results with Comparison to Zero Mass Theory

The recorded time histories of kite trajectories were compared with the theoretical predictions derived using the implementation of the zero mass theory from Eq. (22). Figure 16 shows an experimentally recorded three-dimensional path plot for a horizontally orientated figure of eight maneuver. The corresponding time histories, together with theoretical predictions derived using the zero mass model, are presented in Fig. 17. These are a) position of the kite in terms of azimuth and elevation, b) boundary-layer corrected apparent wind velocity determined using the cup anemometer located proximal to the tether, c) measured onset velocity (obtained using ϕ, θ, and V_A as described in Sec. IV.D) and predicted onset

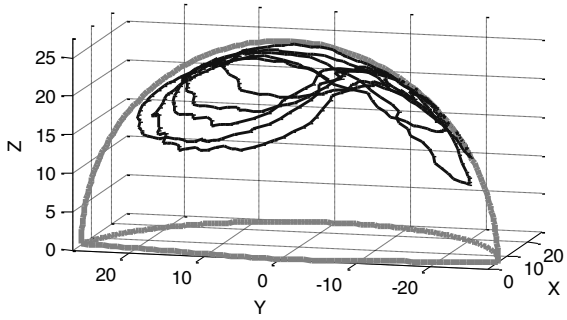

Fig. 16 Three-dimensional path plot for experimentally recorded position angles.

velocity [using the zero mass Eq. (22)], and d) measured line load (from the load cell) and predicted line line load [using the zero mass Eq. (22) together with Eq. (4)].

Predictions from the zero mass model required experimentally determined quantities to be used as inputs, namely the apparent wind velocity, the measured kite position angles, and the drag angle obtained during static flight measurements. The inputs themselves are subject to the limitations of their measurement. The measurement error for the position angles plotted in Fig. 17 is less than 1.32 deg with 95% confidence, (see Table 4). This corresponds to a percentage error of 0.73% over the full 180 deg range of possible measurement angles.

Position error will arise from making the assumption that the flying line is straight in determination of the kite coordinates because in practice, although small, the drag and weight that act on the flying line will induce line curvature. In the case of the experimental test kite, observation and initial modeling has shown that this is not likely to exceed 1 deg because the forces acting on the line are very small relative to the line tension. By using the position coordinates to determine the kite velocity, errors in position that are caused by line curvature do not affect calculated velocities provided the line curvature is unaltered.

Consideration has been given to potential error imposed by the presence of stretch of the test kite flying lines, because in the zero mass model the lines are assumed to be inextensible. Estimates have shown that the degree of added motion caused by line stretch and subsequent recoil is sufficiently small that it can safely be neglected without significant detriment to the results.

The apparent wind during dynamic tests is not constant but is subject to natural variations in wind strength as displayed in Fig. 17b. Changes in direction are also likely to be present, although these are not directly measured in the current study. It is assumed that the wind direction is steady, based on the FE definition of Sec. IV.C.1. Additional wind velocity errors are imposed by the spatial and temporal difference between the anemometer and the kite. That is to say, the anemometer measures the wind at one fixed position in space, and the kite traverses a variety of positions of differing horizontal and vertical extent, not all of which are accurately accounted for by application of Eq. (6) used to correct for the effect of the Earth's boundary layer. Consideration of the rate of change of wind velocity, together with maximum spatial separation of the kite and the anemometer suggests that a maximum error of 20% can be realized for the measurement of the apparent wind at the static kite.

In Fig. 17c, the experimentally obtained onset velocities are compared with those predicted theoretically using the zero mass model and are seen to correlate well.

The measured and theoretical load is compared in Fig. 17d. The load cell measurement has been shown to be to within 24.0 N of the true load with 95% confidence (see Table 5). Expressing this as a percentage of the calibrated load range yields a measurement error of 1.36%. It is seen that for the most part, the line tension predictions compare favorably to the measured results. In a few instances, the line tension is both overpredicted and underpredicted, such as in the period 15 s < time < 20 s. This is thought to be due to the aforementioned difficulties in capturing the true variation in the wind at the point of the kite.

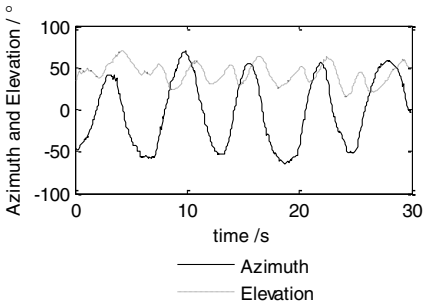

a)

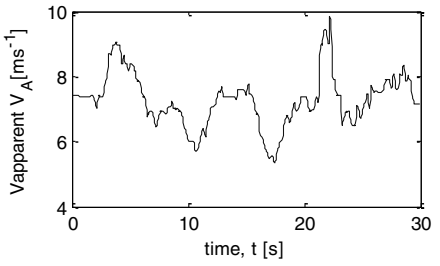

b)

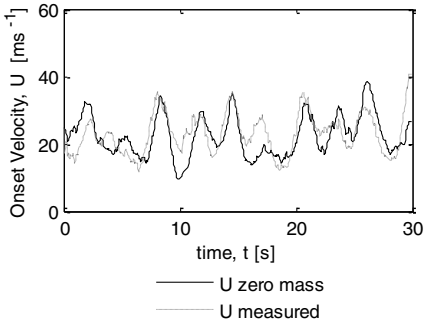

c)

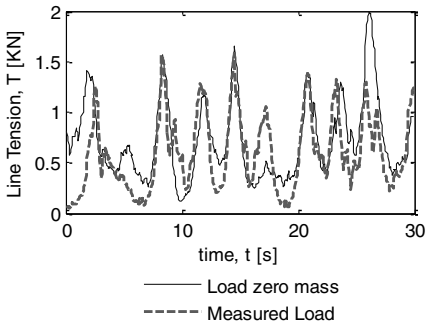

d)

Fig. 17 Time histories for a figure of eight maneuver.

Taking a possible maximum wind measurement error of 20%, the error in lift can be developed from Eq. (2) as

$$L \propto (U+\delta)^2$$

$$\frac{L'-L}{L} = \frac{\frac{1}{2}\rho A C_L(2U\delta+\delta^2)}{L} = \frac{2U\delta+\delta^2}{U^2}$$

$$= 2\left(\frac{\delta}{U}\right) + \left(\frac{\delta}{U}\right)^2 = 0.44$$

This illustrates that a 20% difference between the true onset velocity and the theoretically predicted onset velocity leads to an

Table 4 Statistical quantities for potentiometer accuracy

Number of samples	375
Mean absolute error	1.11 deg
Standard deviation	0.673 deg
95% confidence interval (for one sample)	1.32 deg
99% confidence interval (for one sample)	1.73 deg

Table 5 Statistical quantities for load cell accuracy

Number of samples	60
Mean absolute error	10.1 N
Standard deviation	12.3 N
95% confidence interval (for one sample)	24.0 N
99% confidence interval (for one sample)	31.7 N

estimated 44% difference between the measured and the theoretical lift. This tends to imply that high-quality results require tests to be conducted using artificially created winds, such as by towing the test rig on a still day. This method removes the spatial and temporal variations in the wind.

VI. Conclusions

A test rig for measuring kite performance has been developed. New experimental methods have been established that are suitable for measurement of static flight performance characteristics and for recording dynamic flight time histories. Measurement error has been shown to be less than 1.32% for kite position angles and 1.36% percent for load measurement over the operable range, with 95% confidence.

For the test used in the current study, the static performance parameters are shown to be $L/D = 6.07 \pm 0.5$ and $C_L = 0.776 \pm 0.05$. These are established with 95% confidence. It has been shown that higher L/D induces higher onset velocities, favorable to generating line tension but potentially with detriment to favorable stability characteristics.

The zero mass theory has been used to demonstrate that dynamic performance in terms of the kite velocity and line tension can be predicted in a computationally inexpensive way by assuming that the kite is weightless, and that under this assumption L/D and C_L remain constant during dynamic flight. The line tensions during dynamic maneuvers have been predicted using the zero mass theory and are shown to compare favorably with experimental results. In comparing the zero mass model to experiments, there is a reliance on measured quantities for input, namely the wind velocity at the kite, the static flight drag angle, and the kite spherical position coordinates. This requires these quantities to be measured as accurately as possible. Through analysis of potential errors, it is likely that the most significant error affecting kite performance predictions is that caused by the spatial variability in the wind between the kite and the anemometer itself. Although these can be desirably reduced by making corrections, these are most effectively eliminated by conducting testing on still air days while generating the required apparent wind strength through a steady tow velocity.

The kite flies such that it seeks a natural velocity that is determined by the zero mass theory, although in the presence of mass it may not be achieved exactly. The significance of the assumptions that the kite and lines are weightless, and that L/D and C_L remain constant during dynamic flight, have been assessed by comparison to a new lumped mass model that considers mass and allows L/D and C_L to be freely determined. It has been demonstrated that in the limit where $M = 0$, the two adopted models produce identical results. For a kite of light construction, kite mass modifies flight so that L/D and C_L only vary slightly and thus can be assumed to remain constant at their static flight values to obtain a reasonable engineering approximation to kite flight. If the construction of the kite and lines is such that the weight is larger in comparison to the aerodynamic forces generated, then the lumped mass model is likely to be necessary to predict variations in L/D and C_L and thus kite performance.

Appendix 1: System Calibration

I. Load Transducer Calibration

The load on the arm was systematically increased using several 20 kg hanging masses. To obtain maximal resolution, the amplifier gain and zero settings were adjusted so that the loads ($0 <$ load$<$ 200 kg) produce an output ($-5 < V < 5$) that closely matched the full range of the analog-to-digital card. Loads are hence discretized into the largest possible number of bits (4096) for maximum resolution. The system is rezeroed before each test or calibration to offset drift caused by small changes in the electrical or physical properties of the system. A high-value 180 kg is established and the corresponding reading, in bits, is captured using acquisition software. Then a low-value 0 kg is established and the corresponding reading is captured. A 10 s average is used at a capture frequency of 10 Hz to remove the introduction of error due to noise. A straight line curve (in the form Load = 'rate' × 'bits' + constant) is fitted to allow conversion of the recorded data in bits to the desired load.

II. Potentiometer Calibration

Using a similar process to that of the load cell calibration, the amplifier output voltage is adjusted to fall within the usable range of the AD card. The arm is set to its mid position, 0 deg, using a digital protractor (model PRO 3600) with a resolution of 0.01 deg. The amplifier zero is adjusted to produce a midrange reading of 2048 bits. The arm is then set to −90 deg corresponding to its most-starboard position. The amplifier gain setting is adjusted to set the correct range. A low value of −90 deg and a high value of 90 deg are acquired to complete the calibration. A straight line curve fit is conducted to convert the recorded data in the bits to the desired angle in degrees. Adjustment of arm using the digital protractor is shown in Fig. A1.

III. Experimental Measurement Validation

The results output by the acquisition system are made up of two parts: a portion representing the true value of the measured variable, and another, it is hoped, much smaller portion, representing the combined errors. To interpret the results output by the dynamometer, one has to identify the range of values in which the error could lie. A statistical approach is adopted to identify the accuracy with which measurements can be made with a given confidence limit. Validation of the pitch transducer is identical to that of the yaw transducer.

A. Load Transducer

The calibrated dynamometer is used to take a series of measurements of several exactly defined loads. They are systematically increased and decreased using masses between 0 kg and 180 kg in increments of 20 kg. Each sample is obtained for a capture period of 10 s at 10 Hz, giving rise to a time-averaged measurement. The

Fig. A1 A digital inclinometer is used to set the angle of the arm during calibration.

process is repeated three times to increase the number of samples to 60 in total.

Assuming a normal distribution, the mean and the standard deviations are calculated using standard statistical formulas [38] as well as the 95% and 99% confidence levels. These statistical quantities, presented in Table 5, illustrate the nature of the spread of values about their mean and hence define the accuracy with which measurements can be made.

B. Potentiometer

A procedure similar to that for the load transducer is adopted. A digital inclinometer, accurate to 0.01 deg, is used to define a range of angles between −90 deg and 90 deg at intervals of 45 deg. At each angle, 25 measurements are taken. The process is repeated three times. Table 4 summarizes the statistical quantities based on the combined data of all three sets.

References

[1] Hobbs, S. E., "A Quantitative Study of Kite Performance in Natural Wind with Application to Kite Anemometry," Ph.D. Thesis, Ecological Physics Research Group, Cranfield Inst. of Technology, 1986.

[2] Lansdorp, B., "Design of a 100 MW Laddermill for Wind Energy Generation from Five km Altitude," *7th World Congress on Recovery, Recycling and Reintegration*, Beijing, 2005.

[3] Ockels, W. J., "Laddermill, a Novel Concept to Exploit the Energy in the Airspace," *Aircraft Design*, Vol. 4, Nos. 2–3, 2001, pp. 81–97. doi:10.1016/S1369-8869(01)00002-7

[4] Podgaets, A. R., and Ockels, W. J., "Three-Dimensional Simulation of a Laddermill," *Proceedings of the Third Asian Wind Power Conference*, Wind Power Asia, Beijing, 2006, pp. 116–121.

[5] Loyd, M. L., "Crosswind Kite Power (for Large-Scale Wind Power Production)," *Journal of Energy*, Vol. 4, No. 3, 1980, pp. 106–111. doi:10.2514/3.48021

[6] Wellicome, J. F., "Some Comments on the Relative Merits of Various Wind Propulsion Devices," *Journal of Wind Engineering and Industrial Aerodynamics*, Vol. 20, Nos. 1–3, 1985, pp. 111–142. doi:10.1016/0167-6105(85)90015-7

[7] Williams, P., "Optimal Wind Power Extraction with a Tethered Kite," *AIAA Guidance, Navigation, and Control Conference and Exhibit*, AIAA, Reston, VA, 2006. doi:10.2514/1.30089

[8] Williams, P., Lansdorp, B., and Ockels, W., "Optimal Trajectories for Tethered Kite Mounted on a Vertical Axis Generator," *AIAA Modeling and Simulation Technologies Conference and Exhibit*, AIAA, Reston, VA, 2007.

[9] Williams, P., Lansdorp, B., and Ockels, W., "Optimal Cross-Wind Towing and Power Generation with Tethered Kites," *AIAA Guidance, Navigation and Control Conference and Exhibit*, AIAA, Reston, VA, 2007.

[10] Williams, P., Lansdorp, B., and Ockels, W., "Modeling and Control of a Kite on a Variable Length Flexible Inelastic Tether," *AIAA Modeling and Simulation Technologies Conference and Exhibit*, AIAA, Reston, VA, 2007.

[11] Williams, P., Lansdorp, B., and Ockels, W., "Flexible Tethered Kite with Moveable Attachment Points Part 1: Dynamics and Control," *AIAA Atmospheric Flight Mechanics Conference and Exhibit*, AIAA, Reston, VA, 2007.

[12] Williams, P., Lansdorp, B., and Ockels, W., "Flexible Tethered Kite with Moveable Attachment Points, Part II: State and Wind Estimation," *AIAA Atmospheric Flight Mechanics Conference and Exhibit*, AIAA, Reston, VA, 2007.

[13] Breukels, J., and Ockels, W., "Design of a Large Inflatable Kite Plane," *48th AIAA/ASME/ASCE/AHS/ASC Structures, Structural Dynamics, and Materials Conference*, AIAA, Reston, VA, 2007.

[14] Jackson, P. S., "Optimal Loading of a Tension Kite," *AIAA Journal*, Vol. 43, No. 11, 2005, pp. 2273–2278. doi:10.2514/1.3543

[15] Alexander, K., and Stevenson, J., "A test rig for kite performance measurement," *Proceedings of the Institution of Mechanical Engineers Part B: Journal of Engineering Manufacture*, Vol. 215, No. 4, 2001, pp. 595–598. doi:10.1243/0954405011518412

[16] Alexander, K., and Stevenson, J., "Kite Equilibrium and Bridle Length," *Aeronautical Journal*, Vol. 105, No. 1051, 2001, pp. 535–541.

[17] Stevenson, J., Alexander, K., and Lynn, P., "Kite Performance Testing by Flying in a Circle," *Aeronautical Journal*, Vol. 109, No. 1096, 2005, pp. 269–276.

[18] Stevenson, J. C., and Alexander, K. V., "Circular Flight Kite Tests: Converting to Standard Results," *Aeronautical Journal*, Vol. 110, No. 1111, 2006, pp. 605–614.

[19] Wellicome, J. F., and Wilkinson, S., "Propulsive Kites: An Initial Study," Univ. of Southampton, Rept. SSSU 19, Southampton, England, U.K., 1984.

[20] Naaijen, P., Koster, V., and Dallinga, R. P., "On the Power Savings by an Auxiliary Kite Propulsion System," *International Shipbuilding Progress*, Vol. 53, No. 4, 2006, pp. 255–279.

[21] Bryant, L. W., and Brown, W. S., "Collected Researches on the Stability of Kites and Towed Gliders," National Physics Lab., Rept. 2303, Southampton, England, U.K., 1942.

[22] Wellicome, J. F., and Wilkinson, S., "Propulsive Kites: An Initial Study," Univ. of Southampton, Rept. SSSU 19., Southampton, England, U.K., 1984.

[23] Williams, P., Lansdorp, B., and Ockels, W., "Flexible Tethered Kite with Moveable Attachement Points, Part II: State and Wind Estimation," *AIAA Atmospheric Flight Mechanics Conference and Exhibit*, AIAA, Reston, VA, 2007.

[24] Williams, P., Lansdorp, B., and Ockels, W., "Flexible Tethered Kite with Moveable Attachment Points Part I: Dynamics and Control," *AIAA Atmospheric Flight Mechanics Conference and Exhibit*, AIAA, Reston, VA, 2007.

[25] Williams, P., Lansdorp, B., and Ockels, W., "Modeling and Control of a Kite on a Variable Length Flexible Inelastic Tether," *AIAA Modeling and Simulation Technologies Conference and Exhibit*, AIAA, Reston, VA, 2007.

[26] Williams, P., Lansdorp, B., and Ockels, W., "Optimal Cross-Wind Towing and Power Generation with Tethered Kites," *AIAA Guidance, Navigation and Control Conference and Exhibit*, AIAA, Reston, VA, 2007.

[27] Williams, P., "Optimal Wind Power Extraction with a Tethered Kite," *AIAA Guidance, Navigation, and Control Conference and Exhibit*, AIAA, Reston, VA, 2006.

[28] Wellicome, J. F., and Wilkinson, S., "Propulsive Kites: An Initial Study," Univ. of Southampton, Rept. SSSU 19, Southampton, England, U.K., 1984.

[29] Hobbs, S. E., "A Quantitative Study of Kite Performance in Natural Wind with Application to Kite Anemometry," Ph.D. Thesis, Ecological Physics Research Group, Cranfield Inst. of Technology, 1986.

[30] Claughton, A. R., Shenoi, R. A., and Wellicome, J. F., *Sailing Yacht Design Theory*, 1st ed., Addison Wesley Longman, Reading, MA, 1998, pp. 5–6.

[31] Wellicome, J. F., and Wilkinson, S., "Propulsive Kites-An Initial Study," Univ. of Southampton, Rept. SSSU 19, Southampton, England, U.K., 1984.

[32] MATLAB, MathWorks, Software Package. [Ver. 7.0.0]. 2004. Cambridge, England, U.K.

[33] Tangler, J. L., "Horizontal Axis Wind Turbine Post Stall Airfoil Characteristics Synthesization," Solar Energy Research Inst., SERI/TP-257-4400,, Solar Energy Research Institute, Golden, CO, 1984.

[34] Abbott, I. H., and Doenhoff, A. E., *Theory of Wing Sections*, Dover Publications, New York, 1959.

[35] Hoerner, S. F., "*Fluid Dynamic Drag: Practical Information on Aerodynamic Drag and Hydrodynamic Resistance*," Hoerner Fluid Dynamics, Albuquerque, NM, 1965, pp. 3–9.

[36] Turbo, A. D., Data Aquisition, Software Package. [Ver. 1.0]. 1986. Southampton, Wolfson Unit for Marine Technology and Industrial Eerodynamics.

[37] Wellicome, J. F., and Wilkinson, S., "Propulsive Kites-An Initial Study," Univ. of Southampton, Rept. SSSU 19, Southampton, England, U.K., 1984.

[38] Calvert, J. R., and Farrar, R. A., *An Engineering Data Book*, 2nd ed., Palgrave Macmillan, New York, 1999, pp. 4–5.